Environment and Natural Resources Journal

Volume 23
Issue 6
2025

Selective Adsorption of Cationic Dyes by Hydrochar Derived from *Spirogyra* sp. Algae via Temperature-Varying Hydrothermal Carbonization

Muhammad Badaruddin[1], Laila Hanum[3], Elda Melwita[2,5], Sahrul Wibiyan[2,4], Yulizah Hanifah[6], and Aldes Lesbani[2,4*]

[1]*Environmental Science, Postgraduate Program, Universitas Sriwijaya, Palembang, 30139, South Sumatera, Indonesia*
[2]*Materials Science, Graduate School, Universitas Sriwijaya, Palembang, 30139, South Sumatera, Indonesia*
[3]*Biology Department, Faculty of Mathematics and Natural Sciences, Universitas Sriwijaya, Indralaya, 30662, South Sumatera, Indonesia*
[4]*Research Center of Inorganic Materials and Coordination Complexes, Universitas Sriwijaya, Palembang, 30139, South Sumatera, Indonesia*
[5]*Department of Chemical Engineering, Faculty of Engineering, Universitas Sriwijaya, Ogan Ilir, South Sumatera, 30862, Indonesia*
[6]*National Research and Innovation Agency (BRIN), PUSPIPTEK, Tangerang Selatan, 15311, Indonesia*

ARTICLE INFO

Received: 30 May 2025
Received in revised: 30 Jul 2025
Accepted: 6 Aug 2025
Published online: 16 Sep 2025
DOI: 10.32526/ennrj/23/20250138

Keywords:
Hydrothermal carbonization/ *Spirogyra* sp./ Hydrochar/ Cationic dye selectivity/ Regeneration

*** Corresponding author:**
E-mail:
aldeslesbani@pps.unsri.ac.id

GRAPHICAL ABSTRACT

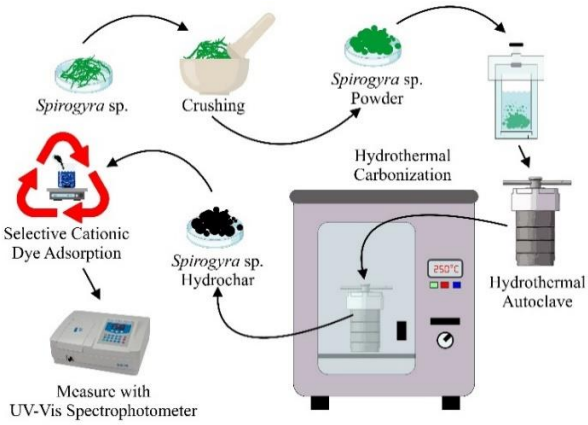

ABSTRACT

This study synthesized hydrochar adsorbents at varying temperatures 150°C (HC150) and 250°C (HC250), using the hydrothermal carbonization (HTC) method from *Spirogyra* sp. (SPG) and characterized them using XRD, FTIR, SEM, and BET analyze. XRD results confirmed a dominant $CaCO_3$ phase (JCPDS 01-086-2334) in all samples, with new peaks and shifts in HC150 and HC250 indicating structural changes from hydrochar formation. FTIR spectra revealed functional groups such as O-H, C=O, C-O, and C-N-S in SPG, with notable reductions in O-H and phenolic signals in HC150 and HC250, suggesting chemical transformations. SEM analysis revealed that SPG exhibits a smooth, sheet-like morphology, while HC150 formed uniform particles and HC250 developed a rough, porous surface, indicating increased carbonization, surface heterogeneity, and enhanced adsorption potential. BET analysis showed a marked increase in surface area and a transition from macroporous to mesoporous structures in HC150 and HC250, enhancing their adsorption capabilities. Adsorbents exhibited selective adsorption toward methylene blue (MB). Surface charge analysis revealed similar pHpzc values slightly below neutral, promoting favorable electrostatic interactions with cationic MB. Adsorption followed pseudo second order (PSO) kinetics compared to pseudo first order (PFO), indicating chemisorption, while isotherm modeling highlighted HC250 strong fit to the Freundlich model. Thermodynamic assessments confirmed HC250 superior performance, exhibiting more negative ΔG, lower ΔH, and higher ΔS values, signifying spontaneous, energy-efficient, and affinity-driven adsorption. Regeneration tests further underscored HC250 stability, with removal efficiency maintaining above 50% after four cycles (90.14% to 53.55%). In comparison, HC150 showed good reusability (80.56% to 51.88%), while SPG declined significantly (56.23% to 50.20%) after two cycles.

HIGHLIGHTS

Hydrochars derived from *Spirogyra* sp. (SPG) were successfully synthesized via hydrothermal carbonization at 150°C (HC150) and 250°C (HC250), and characterized using XRD, FTIR, SEM, and BET. All adsorbents exhibited selective methylene blue (MB) adsorption, with HC250 showing the highest removal efficiency (69.02%) and maximum adsorption capacity (89.29 mg/g). Moreover, HC250 maintained over 50% efficiency after four regeneration cycles, confirming its stability and reusability.

Citation: Badaruddin M, Hanum L, Melwita E, Wibiyan S, Hanifah Y, Lesbani A. Selective adsorption of cationic dyes by hydrochar derived from *Spirogyra* sp. algae via temperature-varying hydrothermal carbonization. Environ. Nat. Resour. J. 2025;23(6):595-611. (https://doi.org/10.32526/ennrj/23/20250138)

1. INTRODUCTION

Water is essential for all living things and life forms; however, its availability is increasingly threatened by limited supply and ever-growing demand (Hamad et al., 2024). Industrial effluents containing synthetic dyes are a considerable environmental challenge (Singh et al., 2024). Synthetic dyes are widely used in various industries, such as chemical, textiles, papermaking, food, printing, plastics, and cosmetics, replacing natural dyes due to their wide availability (Laggoun et al., 2025; Mon et al., 2023; Shi et al., 2022). The waste generated has the potential to pollute the environment (Cui et al., 2025; Ullah et al., 2022). Wastes containing toxic dyes can enter the food chain, increase the risk of health problems in living organisms, are both toxic and carcinogenic, and can form toxic compounds that harm aquatic flora and fauna, negatively impacting human health, such as the risk of mutagenesis, allergies, and cancer (Doondani et al., 2024; Ahmad et al., 2025; Sornaly et al., 2024). Its complex chemical structure makes it highly physically, chemically, thermally, and optically stable, making it difficult to degrade by chemicals, microbial enzymes, oxidizing agents, or heating, causing difficulties in textile industry wastewater treatment (Kumar et al., 2021). Coagulation (Ren et al., 2022), filtration (Norrahma et al., 2023), phytoremediation (Wibowo et al., 2023), electrochemical degradation (Ganash et al., 2024), photodegradation (Kala et al., 2024), and adsorption (Wang et al., 2024) are some methods for reducing the pollution caused by the dye. Adsorption is frequently employed because it is thought to have benefits such as high effectiveness, ease of use, low cost, and environmental safety (Lesbani et al., 2024; Umesh et al., 2024).

Activated carbon was employed as a dye adsorbent in earlier research. However, because it uses bases or acids to activate the adsorption active sites, which may affect the environment, activated carbon has a less environmentally friendly process (Neme et al., 2022). Accordingly, recent research has focused on cost-effective and eco-friendly biomass adsorbent technologies including hydrothermal carbonization (HTC) (Badaruddin et al., 2025). One of the best thermochemical methods for treating biomass with a high moisture content is hydrothermal carbonization. In order to transform the biomass into a solid that is rich in carbon namely hydrochar, the method involves thermally breaking down natural feedstock biomass in an aqueous medium at mild conditions to induce dehydration and decarboxylation processes (Spagnuolo et al., 2023).

Hydrochar is an effective and economical adsorbent for dyes due to its highgly porous structure. In addition, hydrochar is porous, eco-friendly, affordable, and rich in functional groups (González-Fernández et al., 2024; Le et al., 2025; Normah et al., 2022). Previous studies using rambutan peel (Normah et al., 2021), longan fruit (Palapa et al., 2023), and algae (Arora et al., 2024) have identified potential sources of raw materials that can be be converted into hydrochar, which is a more valuable product used in various applications such as dye adsorbent. Algae are effective adsorbents for dyestuffs because the hydrochar produced has a high adsorption capacity without the need for additional activation and its hydrothermal process synthesis is environmentally friendly. The nitrogen groups in the hydrochar also strengthen the bond with the adsorbate, making it an efficient and sustainable solution for dye wastewater treatment (Spagnuolo et al., 2023). According to previous research by (Badaruddin et al., 2025), hydrochar algae *Spirogyra* sp. has a greater adsorption capacity than its raw form which amounts to 34.96 mg/g to 99.01 mg/g when used to adsorbed malachite green dye. Research by (Wijaya et al., 2025), using *Spirogyra* sp. algae which used the anionic dye remazol red as an adsorbate showed the maximum capacity of NiCr-LDH composited with *Spirogyra* sp. algae increased from 11.976 mg/g to 47.170 mg/g.

Spirogyra sp. is a green algae with high potential as a cationic dye adsorbent. These algae were chosen due to their abundant availability, low cost, and high carbohydrate content as a carbon source. Algae *Spirogyra* sp. has been a topic of several studies due to its variety of applications. *Spirogyra* sp. cell wall is composed of several layers that contain various polysaccharides, including cellulose, pectin, and algaenan. Pectin, particularly low-methylated homogalacturonan, lends flexibility, whereas cellulose gives structure. Durability is increased by algaenan, a heteropolymer that is extremely resistant to acids and bases. The outer layers also contain xyloglucans and arabinogalactans. In combination, these elements support the ductility and resilience of the *Spirogyra* sp. cell wall (Permann et al., 2022). Research has demonstrated that *Spirogyra* sp. algae may be used as bioindicators for the presence of heavy metal contamination (Chand and Vanavana, 2022). *Spirogyra* sp. is effective in adsorbing Cu, Cd, and Pb,

and grows optimally at 20-25°C (Vetrivel et al., 2017). *Spirogyra* sp. contains a carbohydrate content of 55.7±2.4% (range 42.8-62.0%), making it an excellent raw material for hydrochar synthesis (Tipnee et al., 2015). With this ability, the algae has the potential not only as a heavy metal biosorbent, but also as a cationic dye adsorbent in industrial wastewater treatment.

Based on these data, this study used *Spirogyra* sp. algae carbonized into hydrochar by hydrothermal method for selective adsorption of cationic dyes (rhodamine b, malachite green, methylene blue). It is expected to increase the adsorption capacity and structure stability that be used repeatedly and become an environmentally friendly adsorbent.

2. METHODOLOGY

2.1 Chemical and instrumental

Chemicals with analytical reagent purity levels were used in this study as solvents, such as distilled water (H_2O), chemicals such as sodium hydroxide (NaOH, ≥98%, Merck), and hydrochloric acid (HCl, 37% w/w, Sigma-Aldrich). Analytical grade rhodamine b (RB, ≥98%), malachite green (MG, ≥98%), and methylene blue (MB, ≥98%) used in the cationic dye adsorption selectivity tests were purchased from Sigma-Aldrich. The area of Lebung Jangkar Village, Pemulutan Subdistrict, Ogan Ilir Regency, South Sumatra Province, with geographical coordinates of -3.113052°N and 104.786218°E, was the sampling location of algae *Spirogyra* sp.

Analytical tools and common laboratory equipment were used in the experiments. A 100 mL stainless steel hydrothermal autoclave was used for adsorbents synthesis. The *Spirogyra* sp. samples were subjected to a preliminary morphological investigation under a microscope. XRD (Rigaku MiniFlex600) was used to study the crystal structure using Cu-Kα radiation at 2θ = 5° - 80°. FTIR (Shimadzu Prestige-21) was used to identify functional groups in the 4,000-400 cm^{-1} range. SEM (Hitachi SU-3500 & JEOL JSM-IT200, No. BMN) was used to analyze surface morphology and particle size distribution. Using the N_2 adsorption-desorption isotherm at 77 K, BET analysis (Quantachrome NovaWin) was used to calculate the specific surface area, pore size, and volume. A UV-Vis spectrophotometer (EMC-18PC-UV) was used to measure the adsorption efficiency towards the dyes at each dye's distinctive wavelength.

2.2 *Spirogyra* sp. algae pretreatment

After being carefully washed with distilled water, *Spirogyra* sp. algae were examined under a microscope and crushed into small components. The component were crushed and filtered through a 100 mesh sieve after being dried thoroughly in an oven set to 105°C. Following that, XRD, FT-IR, SEM and BET studies were used to analyze the obtained adsorbents (Wibiyan et al., 2024b).

2.3 *Spirogyra* sp. algae carbonization through hydrothermal method

50 mL of distilled water and 2.5 g of *Spirogyra* sp. algae were combined and set in a 100 mL stainless steel hydrothermal autoclave. Following that, the autoclave was heated for 10 h at different temperatures 150°C and 250°C, in the oven. After the heating procedure, the equipment was cooled to room temperature, the adsorbents were washed with distilled water, and dried in an oven at 100°C for 12 h. After being crushed with a mortar and filtered through a 100 mesh sieve, the adsorbents were analyzed with XRD, FT-IR, SEM and BET (Badaruddin et al., 2025; Wibiyan et al., 2023).

2.4 Analysis of the pH of the zero charge point (pHpzc) on the adsorbent

The pHpzc was determined by adding 0.02 g of each adsorbent with 20 mL of 0.1 M NaCl solution that was modified at different pH values from 2 to 11, the pHpzc was determined. A 0.1 M NaOH and HCl solution was used to alter the pH. The mixture was stirred for 24 h, then separated. A pH meter was used to determine the filtrate's final pH, and graphs were used to examine the correlation between the initial and final pH values.

2.5 Selectivity of cationic dye

Rhodamine b, malachite green, and methylene blue cationic dye solutions were made by mixing 10 mL of each dye in a beaker, with concentration values determined at 15 mg/L. during that, the dye mixture was mixed with 0.03 g of adsorbent and allowed to stir for 60 minutes. To measure wavelengths, a UV-visible spectrophotometer was employed. On the selection of cationic dyes. An adsorption efficiency (%) investigation was carried out using Equation 1 to select the selective cationic dyes.

$$\text{Adsorption efficiency (\%)} = \frac{C_0 - C_e}{C_0} \times 100 \quad (1)$$

Where; C_0 represents the initial and C_e represents the remaining concentrations of the dyes mixture in the solution after t minutes of adsorption (mg/L) (Jefri et al., 2025; Wibiyan et al., 2024c).

2.6 Adsorption method

The process of adsorption was carried out by determining variations in pH from 2 to 11, contact time from 0 to 300 min, dye concentration from 30, 40, 50, and 60 mg/L, and temperature from 30, 40, 50, and 60°C was used to optimize the adsorption process. Using a 20 mL methylene blue solution 30 mg/L in variations in pH and 50 mg/L in contact time, the initial concentration was determined using UV-Vis. Before determining the final concentration, 0.02 g of adsorbent was added and stirred for 2 h. HCl and NaOH were used to adjust the pH during the pH variations. Absorbance was measured for time variation at each interval. Utilizing 0.02 g of adsorbent and the ideal contact duration, the effects of temperature and concentration were assessed in a similar manner. To evaluate the adsorption capacity, a mass balance equation was used as shown in Equation 2.

$$q\ (mg/g) = (C_0 - C_e)\frac{V}{m} \quad (2)$$

The dye adsorbed q (mg/g) was calculated from the difference between the initial concentration C_0 (mg/L) and the equilibrium concentration Ce (mg/L), multiplied by the solution volume V (L), and divided by the mass of the adsorbent m (g).

The adsorption kinetics were analyzed using both the pseudo first order and pseudo second order models. The pseudo first order and pseudo second order models are, expressed in Equation 3 and 4.

$$\ln\left(q_e - q_t\right) = \ln q_e - k_1 t \quad (3)$$

$$\frac{t}{q_t} = \frac{1}{k_2 q_e^2} + \frac{t}{q_e} \quad (4)$$

In this equation, q_t (mg/g) is the amount of dye adsorbed at time t (minutes), q_e (mg/g) is the amount adsorbed at equilibrium, and k_1 (1/min) is the rate constant of the first order model and k_2 (g/mg·min) is the rate constant of the pseudo second order model.

Thermodynamic parameters were evaluated to determine the spontaneity and energy changes involved in the adsorption process. The equilibrium constant (KC) was calculated as the ratio of the concentration of adsorbate on the solid phase (CA) to that in the liquid phase (CE), as shown in Equation 5. The Gibbs free energy change ΔG (kJ/mol) was calculated using Equation 6, which incorporates the equilibrium constant (KC), the gas constant R (8.314 J/mol·K), and the temperature T (K). To further determine the enthalpy ΔH (kJ/mol) and entropy changes ΔS (J/mol·K), the van't Hoff equation was applied as shown in Equation 7, where the natural logarithm of KC is plotted against the reciprocal of temperature (1/T).

$$K_C = \frac{C_A}{C_E} \quad (5)$$

$$\Delta G = -RT \ln K_C \quad (6)$$

$$\ln K_C = -\frac{\Delta H}{RT} + \frac{\Delta S}{R} \quad (7)$$

To understand the adsorption equilibrium, both the Langmuir and Freundlich isotherm models were applied. The Langmuir and Freundlich models are described in Equation 8 and 9.

$$\frac{C_e}{q_e} = \frac{1}{K_L q_m} + \frac{C_e}{q_m} \quad (8)$$

$$\ln q_e = \ln K_F + \frac{1}{n}\ln C_e \quad (9)$$

In this model, C_e is the equilibrium concentration, q_e is the amount adsorbed at equilibrium, KL (L/mg) is the Langmuir constant, q_m (mg/g) is the maximum adsorption capacity, KF ((mg/g)(L/mg)$^{(1/n)}$) is the Freundlich constant, and n is the adsorption intensity factor.

2.7 Adsorbent due to regeneration cycles

A beaker was filled with a 20 mL solution of methylene blue dye at a concentration of 50 mg/L, and the pH was adjusted to optimal levels. Subsequently, 0.02 g of adsorbent was added. A magnetic stirrer was used to stir the mixture for 120 min. After that, the adsorbent was separated from the adsorbate. The filtrate, which included the adsorbate, was analyzed for absorbance with a UV-Vis spectrophotometer. The adsorbent was subsequently washed with distilled water and desorbed the assistance of an ultrasonic device. After drying, the adsorbent was prepared and disposed for reuse in the continuing adsorption cycle, using the same method as during the initial adsorption.

3. RESULTS AND DISCUSSION

3.1 Adsorbents characterizat

3.1.1 X-ray diffraction (XRD) characterization analysis

Based on XRD analysis in Figure 1(a), the diffraction patterns of sharp peaks were found and identified in the diffraction patterns of SPG, HC150, and HC250, confirming a good crystalline structure. All of the peaks correspond to JCPDS card 01-086-2334, indicating that calcium carbonate ($CaCO_3$) is the primary phase in all adsorbents. While adsorbents HC150 and HC250 show slight peak shift from 22.99° to 23.28° and the appearance of a new peak at 25.46°, adsorbent SPG shows the main characteristic peaks at 2θ angles of 22.99°, 26.13°, 28.86°, 36.23°, 42.74°, 47.33°, 56.19°, 60.92°, and 65.42. This shows that the hydrochar synthesis procedure generated an insignificant shift in peak site, indicating structural modification or the formation of secondary components, but did not affect the primary crystal structure (Djezzar et al., 2024).

3.1.2 Fourier Transform Infrared (FTIR) spectroscopy characterization analysis

Spirogyra sp. contains polysaccharides such as cellulose, alginic acid, and sulfate, which have ion exchange capabilities and can interact with cationic dye ions through certain functional groups. According to Figure 1(b), *Spirogyra* sp. algae have C-O and C-N-S groups, hydroxyl (O-H), carboxyl (C-H), amine (N-H), and carbonyl (C=O). About 3,400 cm^{-1} (O-H), 2,932 cm^{-1} (C-H), 1,640 cm^{-1} (C=O and COOH), 1,535 cm^{-1} (C-H), 1,020 cm^{-1} (C-O), and 528 cm^{-1} (C-N-S) were identified as the positions of absorption bands (Susanti et al., 2023). Peaks 3,400 cm^{-1}, 2,932 cm^{-1}, 1,640 cm^{-1}, 1,020 cm^{-1}, and 528 cm^{-1} reduced in HC150 and HC250, indicating a decrease in hydroxyl functional groups originating from water content or phenolic N-H groups. This suggests that the process of hydrochar synthesis was successful (Tsarpali et al., 2022).

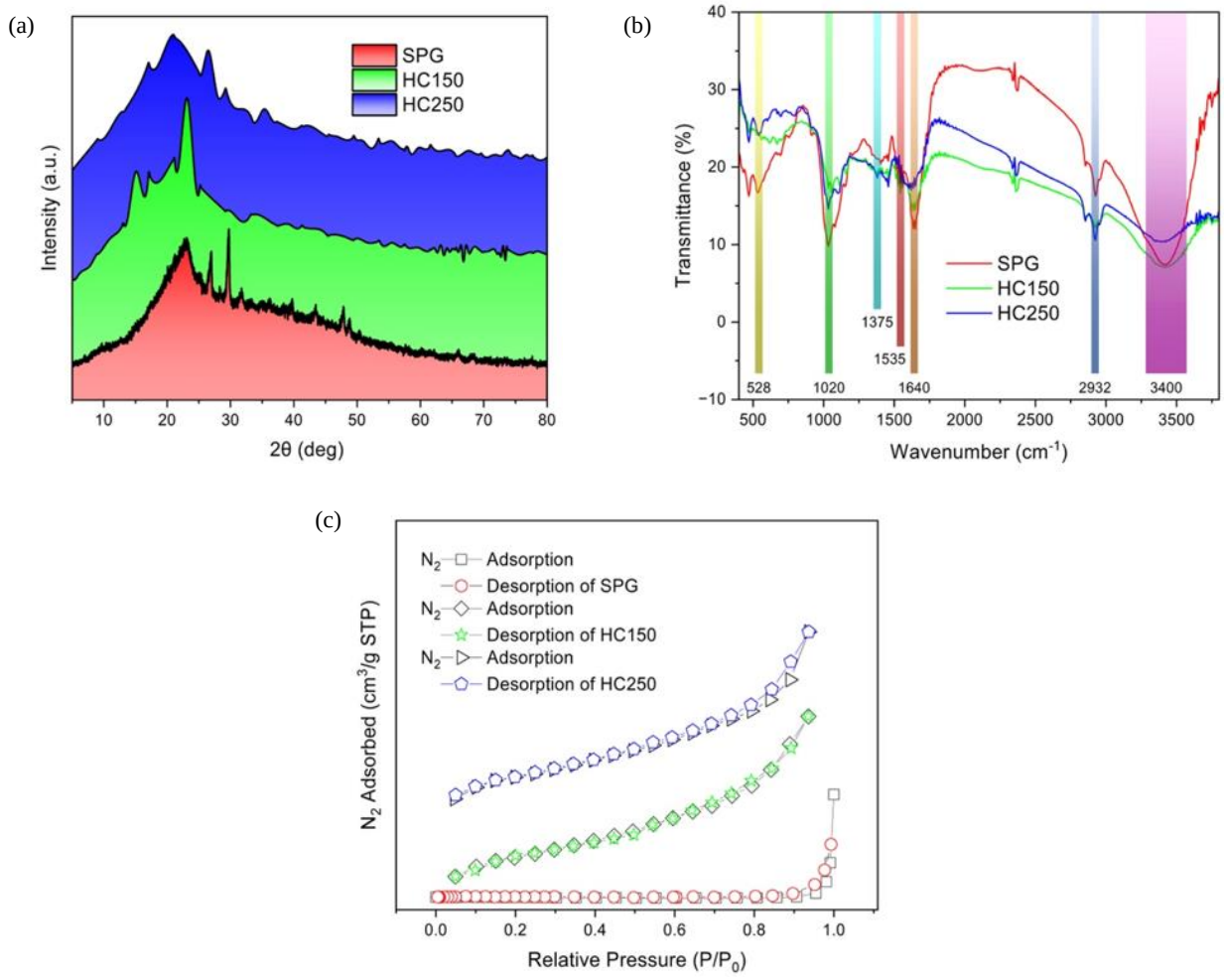

Figure 1. The characterization result of XRD (a), FTIR (b), and BET (c) of SPG, HC150 and HC250

3.1.3 Brunauer-Emmett-Teller (BET) surface area and porosity characterization analysis

The shrinking pore size signifies internal restructuring towards a more stable mesoporous configuration suitable for small molecule diffusion. In the context of cationic dye adsorption, this change is particularly beneficial as the larger surface area provides more active sites, while the meso pore size allows diffusion and sorption of methylene blue dye molecules. In addition, adsorbents usually contain surface oxygen groups (such as carboxyl or hydroxyl) that are able to electrostatically interact with cations (Luo et al., 2023).

BET analysis showed at Table 1 and Figure 1(c) that the surface characteristics and pore structure of *Spirogyra* sp. algae underwent significant changes after undergoing the HTC process at HC150 and HC250. Adsorbent SPG has a very low surface area of 0.2 m^2/g, with a very large average pore size of 87.635 nm and a high pore volume of 2.697 cm^3/g, indicating a large porous structure that is inefficient for small molecule sorption. After HTC treatment, the surface area increased sharply to 5.4 m^2/g in HC150 and 5.5 m^2/g in HC250, with the pore size narrowing to the mesoporous range of about 4.4-4.8 nm and the pore volume decreasing drastically to 0.014-0.015 cm^3/g (Gibson et al., 2019; Li et al., 2024). This increase in surface area resulted from the partial decomposition of biomass and removal of volatile compounds during the HTC process, which opened up the pore structure and formed a more active amorphous carbon surface (Yihunu et al., 2019).

Table 1. Surface area (BET), pore size, and average pore volume of SPG, HC150, and HC250

Adsorbents	Surface area BET (m^2/g)	Pore size average (nm)	Pore volume average (cm^3/g)
SPG	0.2	87.635	2.697
HC150	5.4	4.883	0.014
HC250	5.5	4.438	0.015

3.1.4 Scanning Electron Microscopy (SEM) characterization analysis

The surface morphology characterization of SPG, HC150, and HC250 is shown in Figure 2. SEM reveals that SPG has a smooth, sheet-like structure. This relatively flat surface reflects the natural condition of the biomass before being converted into hydrochar. The absence of large pores or structural irregularities indicates that the surface area of SPG is still limited (Siri-anusornsak et al., 2024). After heat treatment, the morphology of HC150 begins to show significant changes with the formation of relatively uniform, separated particles, indicating the initial decomposition process and the formation of a carbon structure. At higher temperatures, the morphology of HC250 changes drastically into a very rough and irregular surface, with numerous cavities and porous structures spread across the surface. This reflects a higher degree of carbonization and adsorbent decomposition, resulting in increased surface porosity and heterogeneity (Badaruddin et al., 2025).

The particle size distribution analysis of HC150 and HC250 from SEM images, as shown in Figures 2(d) and 2(e), reveals significant differences. HC150 particles exhibit a more uniform distribution with an average size of approximately 4.54 µm and a low standard deviation, reflecting a stable and homogeneous structure. In contrast, although HC250 has an average particle size of 4.13 µm, the particle sizes vary more widely, ranging from 0.669 µm to 14.366 µm, with a higher standard deviation and a median lower than the average, indicating particle fragmentation and agglomeration. HC250 has a broader particle size distribution, suggesting the possible formation of more complex porous structures and a larger surface area. The fragmentation and agglomeration processes occurring at higher temperatures are believed to generate more active sites and pores that contribute to the enhanced adsorption capacity. Meanwhile, HC150, with its more uniform size distribution, indicates a more stable structure but with a relatively lower active surface area compared to HC250. Thus, the increase in heating temperature has a positive effect on the adsorption capability of HC250 by promoting the formation of a more reactive and porous morphology (Li et al., 2023).

3.2 Selective adsorption study of cationic dyes using synthesized adsorbents

Adsorbents SPG, HC150 and HC250 were tested on the selectivity of cationic dyes referring to the ability of the adsorbent to selectively separate

certain dyes from the mixture (Wibiyan et al., 2024a). The cationic dyes mixture in Figure 3 has overlapping wavelengths, which requires spectral deconvolution to figure out the UV-Vis absorption bands. The maximum λ detection accuracy is increased, and overlapping components are successfully identified by using Gaussian fitting (Tones et al., 2020).

Based on the deconvolution curve in Figure 3 and the adsorption efficiency data at Table 2, it can be concluded that all adsorbents used including SPG, HC150, and HC250, have a selective tendency towards MB compared to other cationic dyes. This is indicated by the highest adsorption efficiency of MB adsorption by all adsorbents 39.13% for SPG, 69.29% for HC150, and reached 78.53% for HC250.

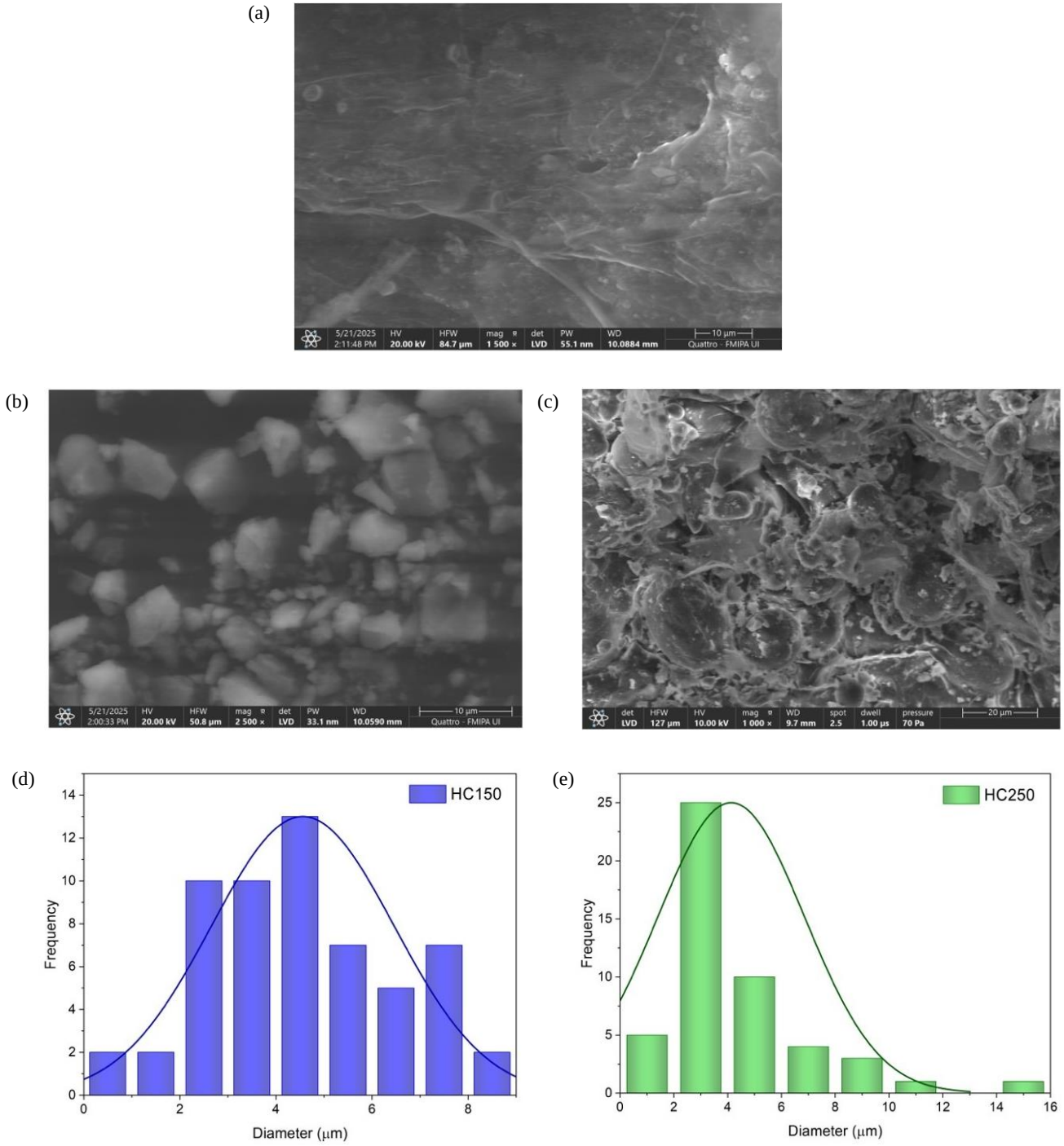

Figure 2. SEM images of SPG (a), HC150 (b), and HC250 (c), with particle distribution graphs of HC150 (d) and HC250 (e)

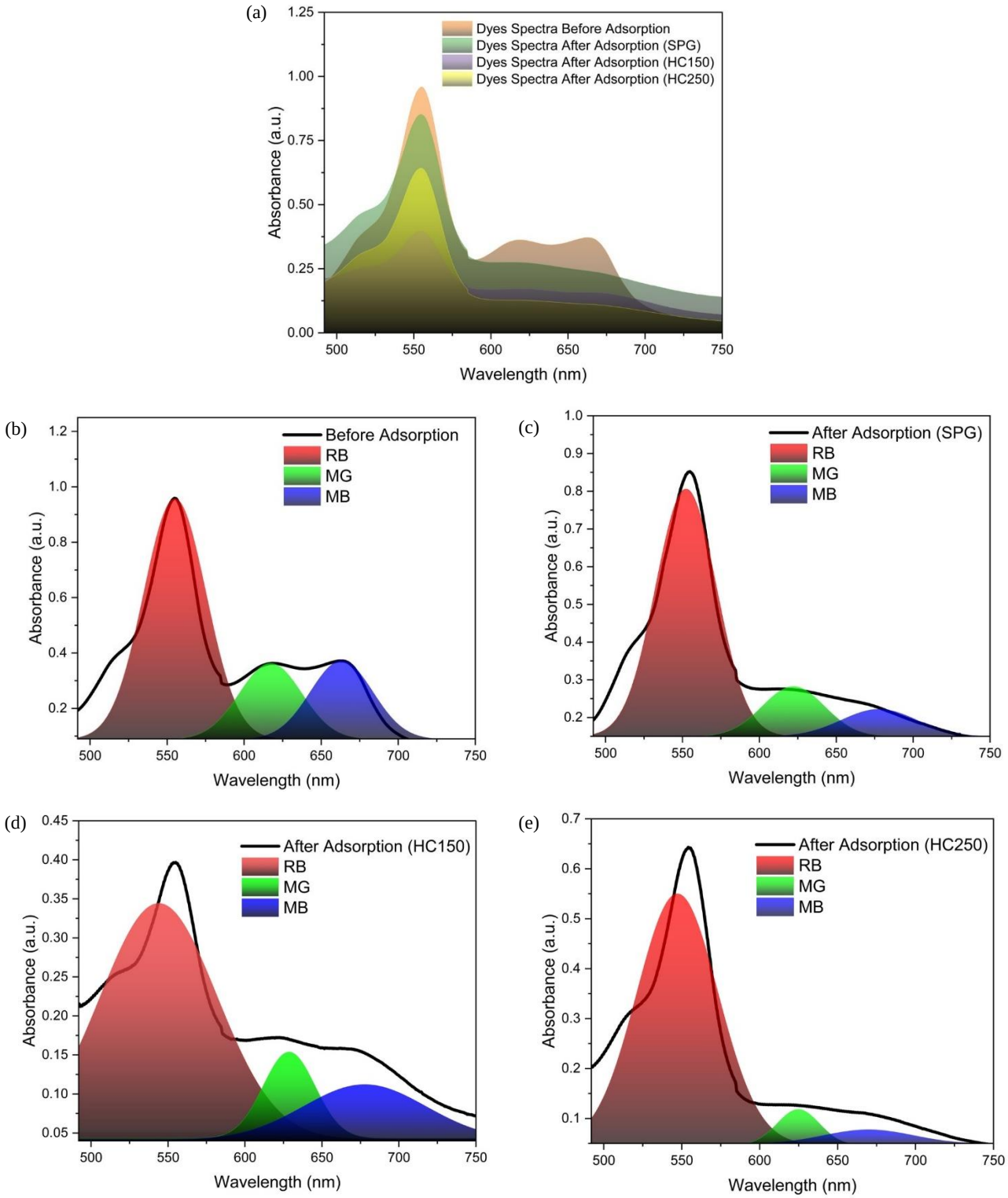

Figure 3. Combined spectra of cationic dye before and after adsorption (a); deconvolution curve of the initial spectrum before adsorption (b); after adsorption by Spirogyra sp. (SPG) (c); after adsorption by HC150 (d); and after adsorption by HC250 (e)

Table 2. The adsorption efficiency of cationic dyes Selectivity by SPG, HC150 and HC250

Dyes	Adsorption efficiency (%)		
	SPG	HC150	HC250
RB	16.35±1.03	64.17±1.18	42.81±1.03
MG	22.40±1.16	57.92±1.16	67.21±0.77
MB	39.13±1.15	69.29±0.77	78.53±0.38

This trend indicates that the structure and chemical properties of MB, such as molecular size, charge, and affinity to active groups on the adsorbent surface, are more compatible with all adsorbents. MB has a planar structure with amine and aromatic groups that allow for stronger π-π interactions and electrostatic bonds with the adsorbent surface, especially if the surface has negatively charged groups or pores of suitable size. In addition, HTC modification of HC150 and HC250 seems to improve the physicochemical properties of the adsorbents, such as surface area and pore regularity, which ultimately contributes to the improved selectivity towards MB (Khan et al., 2022; Wu et al., 2024).

3.3 Adsorption study on pH parameters

The pH of the adsorbents point zero charge is indicated by the pHpzc. The pHpzc values of adsorbents SPG, HC150, and HC250, as shown in Figure 4(a), are 6.60, 6.36, and 6.47, respectively. These values are below the optimum pH value at 7, as shown in Figure 4(b), which explains the way the negatively charged hydroxyl functional groups on the adsorbents surface interact with the MB positive sites. This electrostatic attraction facilitates the adsorption of MB molecules onto the adsorbents surface. Additionally, the relatively close pHpzc values suggest similar surface charge characteristics among the samples, indicating that surface modification only slightly alters their overall charge behavior under near-neutral pH conditions (Wierzbicka et al., 2022).

3.4 Adsorption study on kinetics parameters

Based on the Figure 5 and Table 3, analysis of MB adsorption kinetics with an optimum time of 120 minutes shows that the PSO model fits better than the PFO model for adsorbents SPG, HC150, and HC250.

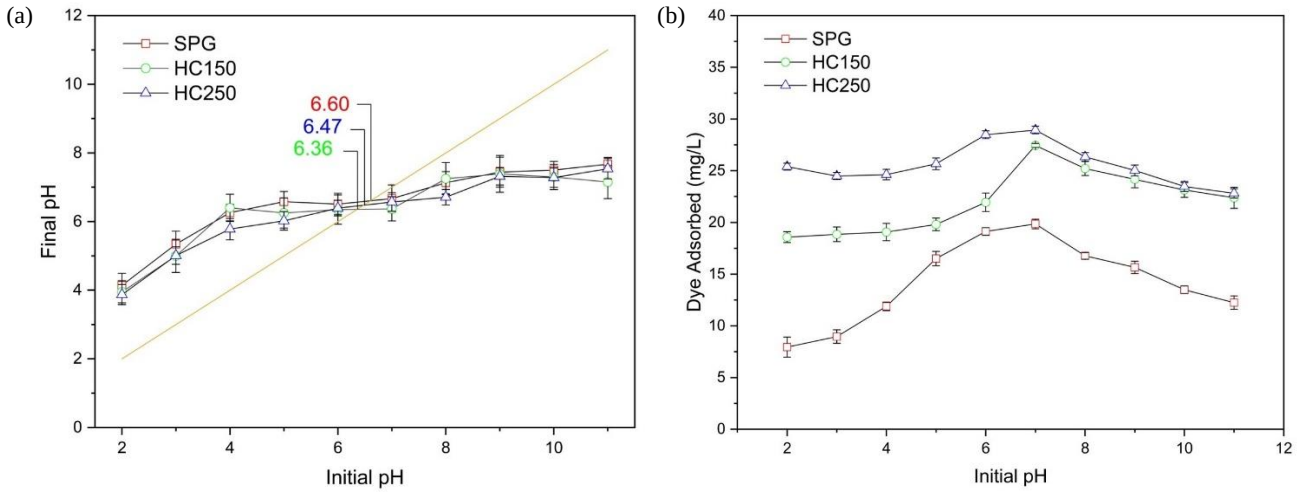

Figure 4. The pHpzc of adsorbents (a), and adsorption variations with pH (b) of SPG, HC150, and HC250

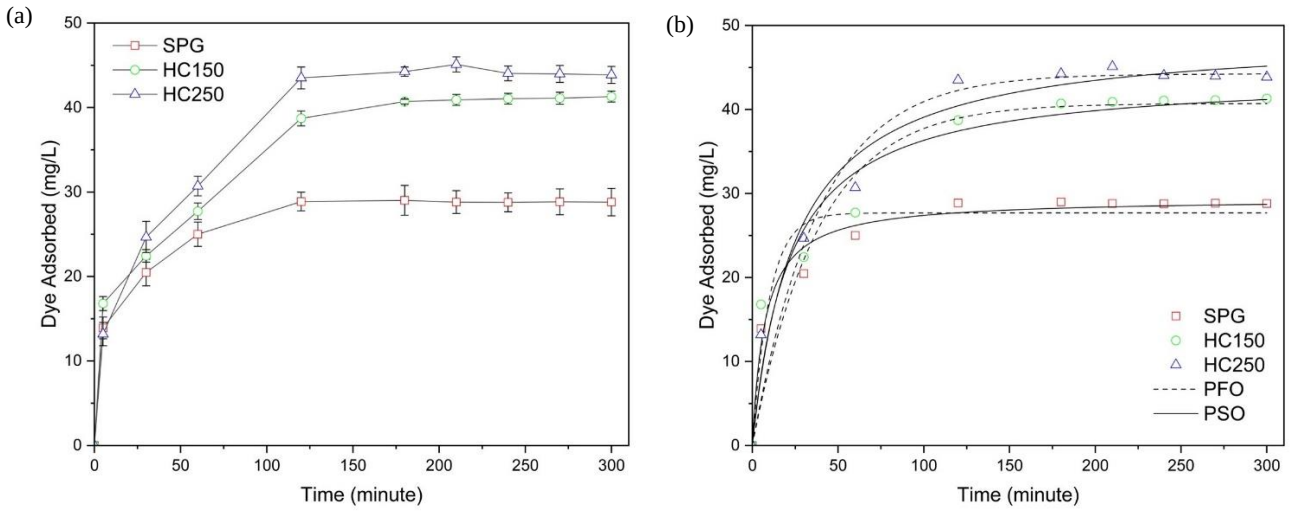

Figure 5. Adsorption vs. contact time (a), and kinetic curves of PFO and PSO Models for SPG, HC150, and HC250 (b)

This is indicated by the very high coefficient of determination (R^2) values in model (≥0.993), compared to the lower PFO between 0.851-0.937. In addition, the Qe_{calc} of the PSO model is closer to the Qe_{exp} value, such as in adsorbents SPG, HC150 and HC250 with Qe_{exp} 28.87, 38.72 and 43.51 mg/g and Qe_{calc} 29.59, 43.48, and 46.73 mg/g, respectively. These results indicate that the adsorption mechanism of MB follows PSO kinetic model, which involves a chemisorption process (Palapa et al., 2025). The increase in adsorption capacity on HC150 and HC250 also suggests that thermal treatment improved the adsorbent performance (Krishna Murthy et al., 2020; Lu et al., 2021).

Table 3. The kinetic parameters of the PFO and PSO models of SPG, HC150, and HC250

Adsorbent	Qe exp (mg/g)	PFO			PSO		
		Qe calc (mg/g)	k_1 (min^{-1})	R^2	Qe calc (mg/g)	k_2 (g/mg)/min	R^2
SPG	28.87	22.24	0.03	0.937	29.59	0.005	0.999
HC150	38.72	30.13	0.02	0.851	43.48	0.001	0.993
HC250	43.51	37.18	0.02	0.937	46.73	0.001	0.993

3.5 Adsorption study on isotherm and thermodynamics parameters

Adsorption isotherms are essential for explaining adsorbent-adsorbate interactions and designing industrial processes, as they reflect adsorbent performance at equilibrium (Eltaweil et al., 2020). They depend on the adsorbent, adsorbate, and solution properties such as temperature, pH, and ionic strength (Mohadi et al., 2023a; Mohadi et al., 2023b; Priatna et al., 2023). According to the Langmuir model Qe_{max} values that shown at Table 4, HC250 had the highest adsorption capacity when compared to HC150 and SPG. At 60°C, the HC250 Qe_{max} decreased to 89.29 mg/g from 125 mg/g at 30°C. At 50°C, HC150 Qe_{max} reached a maximum of 94.34 mg/g, at higher temperatures, it slightly declined. With a capacity of 62.89 mg/g at 30°C and 53.76 mg/g at 60°C, Adsorbent SPG had the lowest capacity. As the temperature increased, the overall decrease in Qe_{max} suggests an exothermic adsorption process (Al-Ghouti and Da'ana, 2020; Ayawei et al., 2017). The R^2 values were higher for the Freundlich isotherm model, indicating a better fit than Langmuir for all adsorbents. All n values of the Freundlich model were above 1, suggesting that the adsorption was favorable and physical in nature. A higher adsorption capacity on heterogeneous surfaces was shown by increased kF values with temperature. A stronger affinity of the adsorbate for the adsorbent surface is indicated by the increasing trend of the kL parameter of the Langmuir model with temperature, particularly in adsorbents SPG and HC250.

Table 4. The Freundlich and Langmuir adsorption isotherms of SPG, HC150, and HC250

Adsorbent	T (°C)	Langmuir			Freundlich		
		Qe_{max}	kL	R^2	n	kF	R^2
SPG	30	62.89	0.037	0.896	1.687	4.528	0.951
	40	60.98	0.044	0.933	1.772	5.212	0.967
	50	56.50	0.057	0.902	1.960	6.464	0.931
	60	53.76	0.077	0.891	2.251	8.478	0.925
HC150	30	77.52	0.138	0.922	1.949	13.72	0.944
	40	89.29	0.119	0.973	1.747	13.08	0.984
	50	94.34	0.111	0.957	1.684	12.78	0.984
	60	85.47	0.134	0.838	1.788	13.75	0.925
HC250	30	125	0.107	0.898	1.493	14.65	0.989
	40	119	0.119	0.840	1.538	15.39	0.975
	50	92.59	0.190	0.837	1.785	18.03	0.945
	60	89.29	0.206	0.807	1.820	18.43	0.923

Table 5 shows the adsorption thermodynamic parameter of SPG, HC150, and HC250. Among the three, HC250 demonstrated thermodynamic superiority in the adsorption process. The most negative ΔG values across the entire temperature range (30-60°C) indicated that the adsorption on HC250 was the most spontaneous, reflecting the strongest adsorbate-adsorbent affinity among the samples. Although the ΔH value of HC250 (3.11 kJ/mol) is lower than HC150 (6.40 kJ/mol) and SPG (7.47 kJ/mol), this indicates that HC250 requires less energy from the environment for adsorption to take place, making it more energy efficient. In addition, the higher ΔS value of HC250 than SPG indicates that adsorption still causes increased disorder at the solid-liquid interface, which favors an effective adsorption mechanism. In summary, the combination of spontaneity (most negative ΔG), energy efficiency (lowest ΔH), and increased interfacial disorder (higher ΔS) establishes HC250 as the most thermodynamically advantageous adsorbent in this system (Krishna Murthy et al., 2020).

Table 5. Adsorption thermodynamic parameter of SPG, HC150 and HC250

Adsorbent	Concentration (mg/L)	ΔH (kJ/mol)	ΔS (kJ/mol)	ΔG (kJ/mol)			
				30°C	40°C	50°C	60°C
SPG	60	7.47	0.026	-0.277	-0.532	-0.788	-1.044
HC150	60	6.40	0.033	-3.629	-3.960	-4.291	-4.622
HC250	60	3.11	0.027	-5.183	-5.456	-5.730	-6.004

3.6 Regeneration cycles study

The regeneration data shown in Figure 6 indicate that adsorbents SPG, HC150, and HC250 experienced a decrease in adsorption efficiency as the cycles of use increased. In the first cycle, the adsorption efficiency of each adsorbent was 56.23% for SPG, 80.56% for HC150, and 90.14% for HC250. Adsorbent SPG was only able to maintain an efficiency above 50% until the second cycle (50.20%), while HC150 and HC250 showed better performance, with efficiencies above 50% until the fourth cycle, which were 51.88% (HC150) and 53.55% (HC250), respectively. This indicates that HC150 and HC250 have higher regeneration stability than SPG. HC250 consistently showed the highest adsorption efficiency in each cycle, indicating that the synthesis of hydrochar with HTC of a certain temperature variations has different characteristics in the adsorbent and more effective in maintaining adsorption capacity after multiple reuses. The main advantage of HC150 and HC250 over SPG lies in their ability to effectively maintain high adsorption efficiency over more reuse cycles.

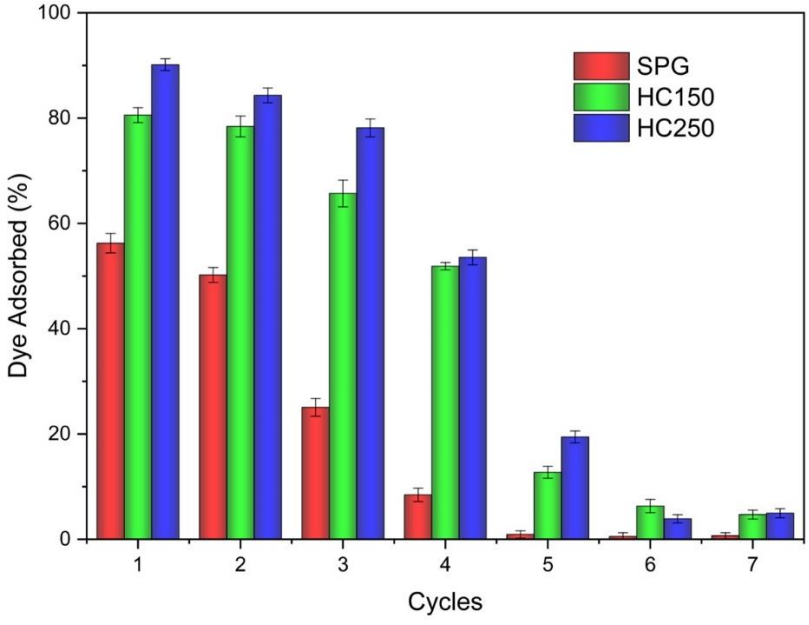

Figure 6. Regeneration cycles of SPG, HC150 and HC250

3.7 Adsorption mechanism study

The comparison of the FTIR spectra before and after MB adsorption of SPG, HC150 and HC250 shown in Figure 7, reveals significant changes in the surface functional groups of SPG, as well as HC150 and HC250, indicating the active involvement of these groups in the adsorption process. The observed decrease in intensity around 3,412 cm^{-1} across all materials suggests the participation of hydroxyl and amine groups through hydrogen bonding or electrostatic interactions with the positively charged MB molecules. Furthermore, shifts and intensity changes at 1,645 and 1,531 cm^{-1}, corresponding to carbonyl and phenolic groups, particularly in SPG and HC150, further support the occurrence of specific interactions between polar functional groups of the adsorbents and MB.

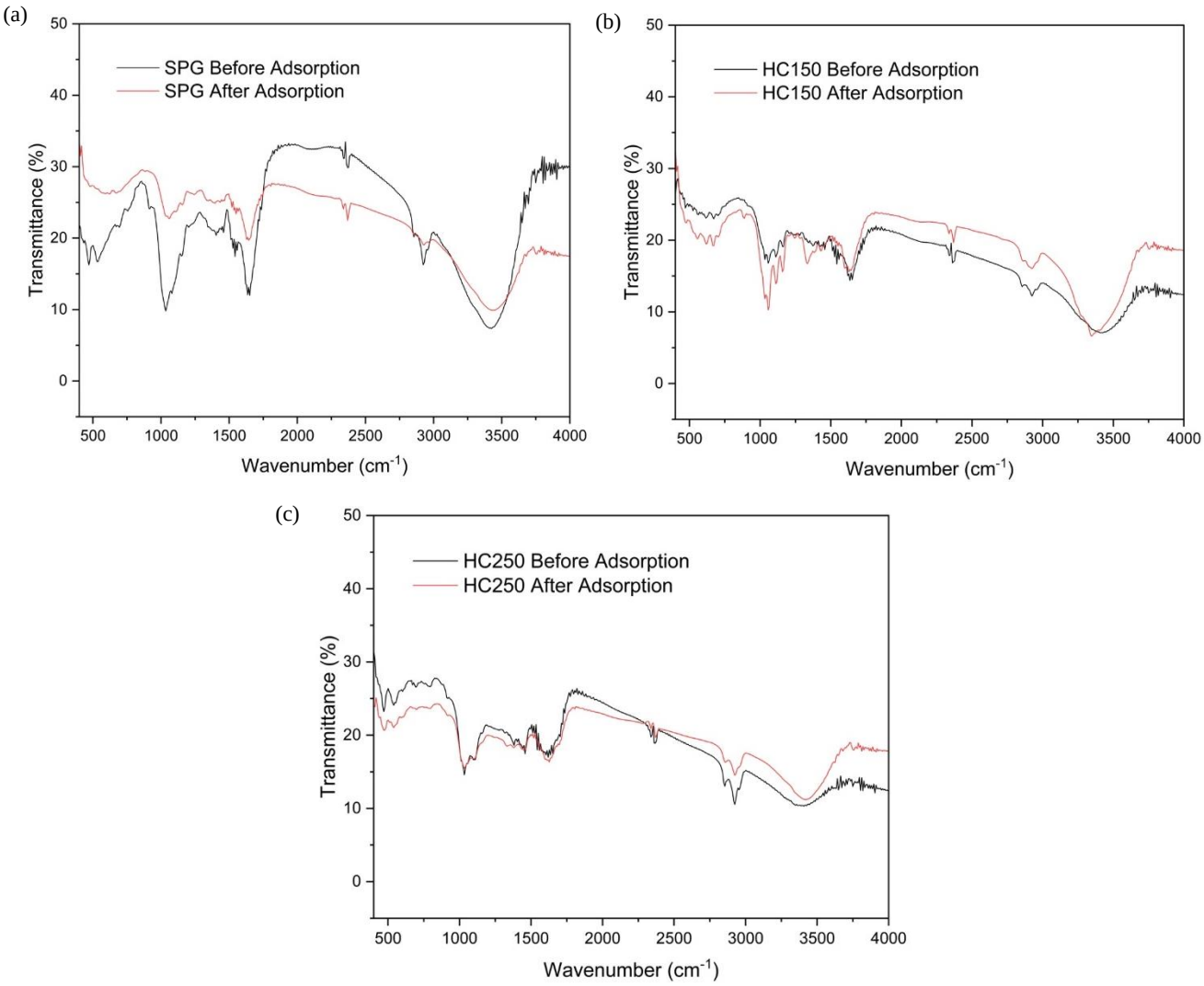

Figure 7. Comparative FTIR spectra of SPG (a), HC150 (b), and HC250 (c) before and after MB adsorption

Additionally, changes in the spectral region between 1,000-500 cm^{-1}, especially involving C-O, C-N, and C-N-S vibrations, indicate possible direct interactions between MB functional groups and the adsorbent surface. Notably, HC250 exhibited fewer spectral changes compared to SPG and HC150, suggesting that its adsorption mechanism is more dominated by π-π stacking interactions between aromatic domains of the hydrochar and the aromatic rings of MB. Overall, the adsorption of MB onto these materials involves a combination of electrostatic interactions, hydrogen bonding, and π-π stacking, with the degree of carbonization influencing the dominant adsorption mechanism. The possible adsorption mechanism is illustrated in Figure 8.

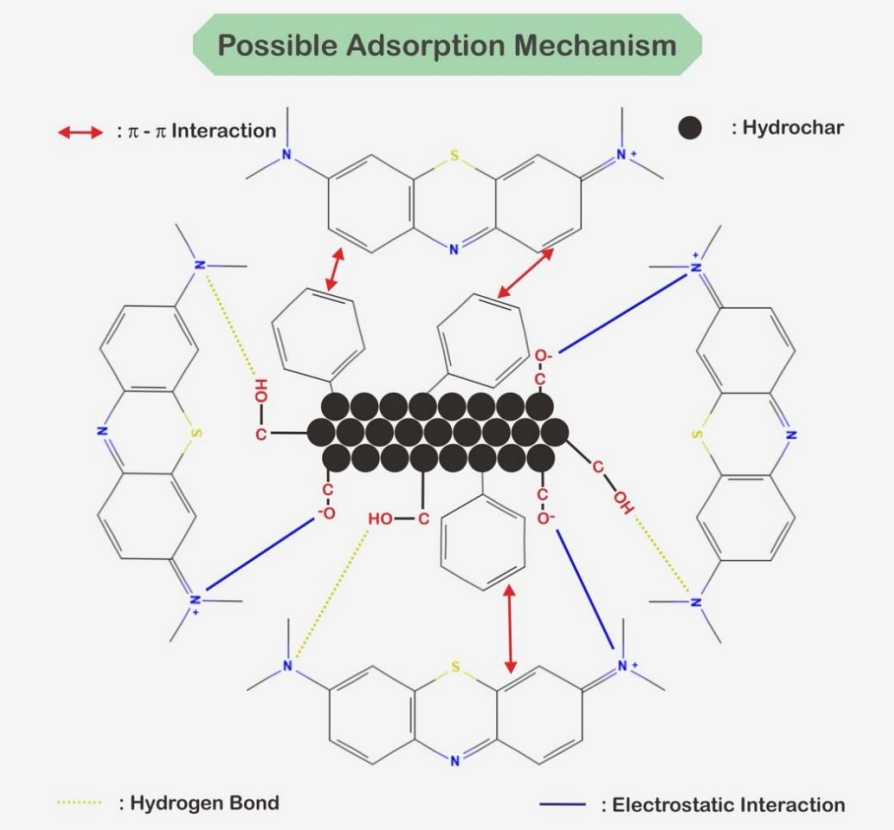

Figure 8. Illustration of the possible adsorption mechanism of MB onto SPG, HC150, and HC250 via electrostatic interaction, hydrogen bonding, and π-π stacking

3.8 Comparison of adsorption capacity of various biomass-based adsorbents for MB adsorption

Table 6 presents a comparison of the adsorption capacities of various biomass-derived adsorbents for MB, synthesized using either pyrolysis or hydrothermal methods. In general, adsorbents produced via the hydrothermal method exhibit higher adsorption capacities compared to those obtained through pyrolysis. For example, biochar derived from *Melia azedarach* fruit and *Chenopodium formosanum*, prepared via pyrolysis, showed adsorption capacities of 25.77 mg/g and 41.16 mg/g, respectively (Karadeniz and Güzel, 2023; Morgan et al., 2025). In contrast, corn straw biochar demonstrated a relatively low capacity of 6.25 mg/g (Zhao et al., 2023). On the other hand, hydrochars synthesized from sunflower stalks and *Shorea* spp. through hydrothermal carbonization achieved higher capacities, reaching 49.37 mg/g and 37.80 mg/g, respectively (Elhassan et al., 2025; Saini et al., 2025). In this study, the hydrochars HC150 and HC250 exhibited even greater adsorption capacities of 85.47 mg/g and 89.29 mg/g, respectively. These results highlight the positive effect of elevated hydrothermal temperatures on the development of surface properties favorable for adsorption. Thus, HC150 and HC250 demonstrate superior performance as adsorbents for MB removal and outperform several other bio-based adsorbents reported in the literature.

Table 6. Comparison of adsorption capacities of various biomass-based adsorbents for MB adsorption

Adsorbents	Methods	Adsorption capacity (mg/g)	References
Biochar from *Melia azedarach* fruit	Pyrolysis	25.77	Karadeniz and Güzel (2023)
Biochar from *Chenopodium formosanum*	Pyrolisis	41.161	Morgan et al. (2025)
Biochar from corn straw	Pyrolisis	6.25	Zhao et al. (2023)
Hydrochar from sunflower stalks (biomass)	Hydrothermal	49.37	Saini et al. (2025)
Hydrochar from *Shorea* spp.	Hydrothermal	37.80	Elhassan et al. (2025)
HC150	Hydrothermal	85.47	This study
HC250	Hydrothermal	89.29	This study

4. CONCLUSION

The successful synthesis of adsorbents SPG, HC150, and HC250 is confirmed through XRD, FTIR, SEM, and BET analyze. XRD analysis confirmed the presence of a dominant $CaCO_3$ crystalline phase (JCPDS 01-086-2334) in all adsorbents, with new peaks and slight shifts in HC150 and HC250 indicating structural changes due to hydrochar synthesis. FTIR spectra showed the presence of O-H, C=O, C-O, and C-N-S groups in SPG, with reduced O-H and phenolic peaks in HC150 and HC250, confirming chemical changes.

SEM analysis confirmed that increasing the carbonization temperature significantly alters the surface morphology and particle distribution of the adsorbents. The raw sample SPG exhibited a smooth, sheet-like surface, while HC150 showed the formation of uniform particles. In contrast, HC250 developed a rough, porous, and heterogeneous structure with broader particle size distribution, indicating advanced carbonization and enhanced potential for adsorption applications.

BET analysis revealed a significant increase in surface area and a shift from macroporous to mesoporous structure in HC150 and HC250, improving their adsorption potential. Adsorbents showed selective adsorption toward MB, with HC250 having the highest removal 69.02%. The study demonstrates that adsorbents possess similar surface charge characteristics, with pHpzc values slightly below neutral, facilitating electrostatic attraction with cationic MB.

Adsorption kinetics follow the PSO model, indicating a chemisorption mechanism with high reliability. Among the adsorbents, HC250 exhibits the best performance, showing the highest adsorption capacity and strong alignment with the Freundlich isotherm model. Thermodynamic evaluations further highlight HC250 superior spontaneity, energy efficiency, and adsorbate affinity, as evidenced by its more negative ΔG, lower ΔH, and higher ΔS values.

Regeneration tests show that HC250 maintains the highest adsorption efficiency across cycles, starting at 90.14% and remaining above 50% through the fourth cycle (53.55%). HC150 also performs well, from 80.56% to 51.88%, while SPG drops from 56.23% to 50.20% by the second cycle. These results confirm that HC250 has the best regeneration stability and reusability among the tested adsorbents.

ACKNOWLEDGEMENTS

We gratefully acknowledge the support provided by the Research Center of Inorganic Materials and Coordination Complexes, Universitas Sriwijaya, in facilitating this research.

AUTHOR CONTRIBUTIONS

Conceptualization: M.B., A.L., L.H., E.M. Data curation: M.B., S.W. Formal Analysis: M.B., S.W., Y,H. Funding acquisition: M.B., A.L. Investigation: M.B., A.L., S.W., Y.H. Methodology: M.B., A.L., L.H., E.M., S.W. Project administration: M.B., A.L., L.H., E.M., S.W. Resources: M.B., S.W. Software: M.B., S.W. Supervision: A.L., L.H., E.M. Validation: A.L., L.H., E.M. Visualization: M.B., S.W. Writing-original draft: M.B., S.W. Writing-review and editing: M.B., A.L., L.H., E.M., S.W.

DECLARATION OF CONFLICT OF INTEREST

The authors declare no conflict of interest.

REFERENCES

Ahmad N, Kameda T, Rahman MT, Rahman F, Lesbani A. Preparation of a new hybrid MgAlLDH@Magnetite activated charcoal by hydrothermal method for stability and adsorption mechanism of congo red. Results in Surfaces and Interfaces 2025;18:Article No. 100440.

Al-Ghouti MA, Da'ana DA. Guidelines for the use and interpretation of adsorption isotherm models: A review. Journal of Hazardous Materials 2020;393:Article No. 122383.

Arora N, Tripathi S, Bhatnagar P, Gururani P, Philippidis GP, Kumar V, et al. Algal-based biochar and hydrochar: A holistic and sustainable approach to wastewater treatment. Chemical Engineering Journal 2024;496:Article No. 53953.

Ayawei N, Ebelegi AN, Wankasi D. Modelling and interpretation of adsorption isotherms. Journal of Chemistry 2017;1:Article No. 3039817.

Badaruddin M, Hanum L, Melwita E, Wibiyan S, Lesbani A. Hydrothermal carbonization of *Spirogyra* sp. algae for adsorption and regeneration of malachite green dye. Chimica Techno Acta 2025;12(1):Article No. 12113

Chand V, Vanavana I. Evaluation of *Spirogyra* Sp. as a bioindicator of heavymetal pollution in a tropical aquatic environment. Pollution Research 2022;41(2):445-50.

Cui C, Qiao W, Li D, Wang L-J. Dual cross-linked magnetic gelatin/carboxymethyl cellulose cryogels for enhanced Congo red adsorption: Experimental studies and machine learning modelling. Journal of Colloid and Interface Science 2025;678:619-35.

Djezzar Z, Aidi A, Rehali H, Ziad S, Othmane T. Characterization of activated carbon produced from the green algae *Spirogyra* used as a cost-effective adsorbent for enhanced removal of copper(ii): Application in industrial wastewater treatment. RSC Advances 2024;14(8):5276-89.

Doondani P, Panda D, Gomase V, Peta KR, Jugade R. Novel chitosan-ZnO nanocomposites derived from Nymphaeaceae fronds for highly efficient removal of Reactive Blue 19, Reactive Orange 16, and Congo Red dyes. Environmental Research 2024;247:Article No. 118228.

Elhassan M, Kooh MRR, Chou Chau YF, Abdullah R. Hydrochar from *Shorea* spp.: A dual-purpose approach for sustainable biofuel and efficient methylene blue adsorbent. Biomass Conversion and Biorefinery 2025;15(4):5779-93.

Eltaweil AS, Ali Mohamed H, Abd El-Monaem EM, El-Subruiti GM. Mesoporous magnetic biochar composite for enhanced adsorption of malachite green dye: Characterization, adsorption kinetics, thermodynamics and isotherms. Advanced Powder Technology 2020;31(3):1253-63.

Ganash A, Othman S, Al-Moubaraki A, Ganash E. An electrodeposition of Cu-MOF on platinum electrode for efficient electrochemical degradation of tartrazine dye with parameter control and degradation mechanisms: Experimental and theoretical findings. Applied Surface Science Advances 2024;19:Article No. 100577.

Gibson N, Kuchenbecker P, Rasmussen K, Hodoroaba VD, Rauscher H. Chapter 4.1 - Volume-specific surface area by gas adsorption analysis with the BET method. In: Characterization of Nanoparticles: Measurement Processes for Nanoparticles. Elsevier; 2019. p. 265-94.

González-Fernández LA, Medellín-Castillo NA, Navarro-Frómeta AE, Castillo-Ramos V, Sánchez-Polo M, Carrasco-Marín F. Optimization of hydrochar synthesis conditions for enhanced Cd(II) and Pb(II) adsorption in mono and multimetallic systems. Environmental Research 2024;261:Article No. 119651.

Hamad N, Galhoum AA, Saad A, Wageh S. Efficient adsorption of cationic and anionic dyes using hydrochar nanoparticles prepared from orange peel. Journal of Molecular Liquids 2024;409:Article No. 125349.

Jefri J, Fithri NA, Ramadhan N. Enhanced selectivity of Ni/Al LDH for cationic dye adsorption via Gambier Leaf Extract Modification. Indonesian Journal of Material Research 2025;3(1):1-7.

Kala K, Vasumathi V, Sivalingam S, Kapali BSC. Optimization of organic dyes photodegradation and investigation of the anticancer performance by copper oxide/graphene oxide nanocomposite. Surfaces and Interfaces 2024;50:Article No. 104482.

Karadeniz F, Güzel F. Adsorptive performance of *Melia azedarach* fruit-derived biochar in removing methylene blue, diclofenac, and copper(II) from aqueous solution. Biomass Conversion and Biorefinery 2023;13(3):2429-47.

Khan I, Saeed K, Zekker I, Zhang B, Hendi AH, Ahmad A, et al. Review on methylene blue: Its properties, uses, toxicity and photodegradation. Water (Switzerland) 2022;14(2):Article No. 242.

Krishna Murthy TP, Gowrishankar BS, Krishna RH, Chandraprabha MN, Mathew BB. Magnetic modification of coffee husk hydrochar for adsorptive removal of methylene blue: Isotherms, kinetics and thermodynamic studies. Environmental Chemistry and Ecotoxicology 2020;2:205-12.

Kumar A, Singh R, Upadhyay SK, Sanjay Kumar S, Charaya MU. Biosorption: The removal of toxic dyes from industrial effluent using phytobiomass: A review. Plant Archives 2021;21(Supplement 1): 1320-5.

Laggoun Z, Khalfaoui A, Derbal K, Ghomrani AF, Benalia A, Pizzi A. Experimental study of selective batch bio-adsorption for the removal of dyes in industrial textile effluents. Journal of Renewable Materials 2025;13(1):127-46.

Le TTU, Ngo TG, Hoang NA, Nguyen VH, Nguyen VD, Hoang LP, et al. Adsorption characteristics of single and binary mixture of methylene blue and rhodamine B of novel hydrochar derived from lemongrass essential oil distillation residue. Journal of Molecular Liquids 2025;425:Article No. 127205.

Lesbani A, Ahmad N, Mohadi R, Royani I, Wibiyan S, Amri, et al. Selective adsorption of cationic dyes by layered double hydroxide with assist algae (*Spirulina platensis*) to enrich functional groups. JCIS Open 2024;15:Article No. 100118.

Li C, Zhong F, Liang X, Xu W, Yuan Q, Niu W, et al. Microwave-assisted hydrothermal conversion of crop straw: Enhancing the properties of liquid product and hydrochar by varying temperature and medium. Energy Conversion and Management 2023;290:Article No. 117192.

Li W, Tao E, Hao X, Li N, Li Y, Yang S. MMT and ZrO_2 jointly regulate the pore size of graphene oxide-based composite aerogel materials to improve the selective removal ability of Cu(II). Separation and Purification Technology 2024; 331:Article No. 125506.

Lu YC, Kooh MRR, Lim LBL, Priyantha N. Effective and simple NaOH-modification method to remove methyl violet dye via *Ipomoea aquatica* Roots. Adsorption Science and Technology 2021;2021:Article No. 5932222.

Luo M, Wang L, Li H, Bu Y, Zhao Y, Cai J. Hierarchical porous biochar from kelp: Insight into self-template effect and highly efficient removal of methylene blue from water. Bioresource Technology 2023;372:Article No. 128676.

Mohadi R, Ahmad N, Wibiyan S, Zahara ZA, Fitri ES, Mardiyanto, et al. Synthesis of Zn/Al-ZnO composite using Zn/Al-layered double hydroxide for oxidative desulfurization of 4-methyldibenzothiophene. Science and Technology Indonesia 2023a;8(4):701-9.

Mohadi R, Palapa NR, Wibiyan S, Mardiyanto, Rohmatullaili, Fitri ES, et al. Catalytic oxidative desulfurization of 4-methyldibenzothiophene by Ni/Al modified titanium dioxide and zinc oxide. Science and Technology Indonesia 2023b;8(3):414-21.

Mon PP, Cho PP, Chandana L, Srikanth VVSS, Madras G, Ch S. Biowaste-derived Ni/NiO decorated-2D biochar for adsorption of methyl orange. Journal of Environmental Management 2023;344:Article No. 118418.

Morgan HM, Jiang TJ, Tsai WT, Yen TB. Initial physiochemical characterization of Djulis (*Chenopodium formosanum*) spent mushroom substrate biochar and its application for methylene blue dye adsorption, isotherm, kinetics, and parameters. Biomass Conversion and Biorefinery 2025;15:19947-61.

Neme I, Gonfa G, Masi C. Activated carbon from biomass precursors using phosphoric acid: A review. Heliyon 2022;8(12):e11940.

Normah N, Juleanti N, Palapa NR, Taher T, Siregar PMSBN, Wijaya A, et al. Hydrothermal carbonization of rambutan peel (*Nephelium lappaceum* L.) as a green and low-cost adsorbent for Fe(II) removal from aqueous solutions. Chemistry and Ecology 2022;38(3):284-300.

Normah N, Juleanti N, Siregar PMSBN, Wijaya A, Palapa NR, Taher T, et al. Size selectivity of anionic and cationic dyes using LDH modified adsorbent with low-cost rambutan peel to hydrochar. Bulletin of Chemical Reaction Engineering and Catalysis 2021;16(4):869-80.

Norrahma SSA, Hamid NHA, Hairom NHH, Jasmani L, Sidik DAB. Industrial textile wastewater treatment using *Neolamarckia cadamba* NFC filter paper via cross-flow

filtration system. Journal of Water Process Engineering 2023;55:Article No. 104188.

Palapa NR, Putra MBK, Musifa E, Yuliasari N, Adawiyah R. Preparation and application of biochar from *Areca catechu* L. peel for malachite green and reactive blue dyes removal. Indonesian Journal of Environmental Management and Sustainability 2025;9(1):28-35.

Palapa NR, Wijaya A, Ahmad N, Amri A, Mohadi R, Lesbani A. Activated hydrochar prepared from Longan Fruit (*Dimocarpus longan* Lour.) peel via hydrothermal carbonization-NaOH activation for cationic dyes removal. Science and Technology Indonesia 2023;8(3):461-70.

Permann C, Gierlinger N, Holzinger A. Zygospores of the green alga *Spirogyra*: New insights from structural and chemical imaging. Frontiers in Plant Science 2022;13:Article No. 1080111.

Priatna SJ, Hakim YM, Wibyan S, Sailah S, Mohadi R. Interlayer modification of west java natural bentonite as hazardous dye rhodamine B adsorption. Science and Technology Indonesia 2023;8(2):160-9.

Ren Y, Liu S, Tan Y, Liu Y, Yuan T, Shen Z, et al. Application of QSAR for investigation on coagulation mechanisms of textile wastewater. Ecotoxicology and Environmental Safety 2022;244:Article No. 114035.

Saini R, Pandey M, Mishra RK, Kumar P. Adsorption potential of hydrochar derived from hydrothermal carbonization of waste biomass towards the removal of methylene blue dye from wastewater. Biomass Conversion and Biorefinery 2025;15(6):9229-49.

Shi Y, Chang Q, Zhang T, Song G, Sun Y, Ding G. A review on selective dye adsorption by different mechanisms. Journal of Environmental Chemical Engineering 2022;10(6)Article No. 108639.

Singh S, Verma N, Umar A, Kansal SK. ZnCdS nanoparticles decorated three-dimensional MoO_3 polygonal structure: A novel photocatalyst for enhanced solar light-driven degradation of methyl orange dye. Journal of Alloys and Compounds 2024;997:Article No. 174714.

Siri-anusornsak W, Kolawole O, Soiklom S, Petchpoung K, Keawkim K, Chuaysrinule C, et al. Innovative use of *Spirogyra* sp. biomass for the sustainable adsorption of Aflatoxin B1 and Ochratoxin A in aqueous solutions. Molecules 2024;29(21):Article No. 5038.

Sornaly HH, Ahmed S, Titin KF, Islam MN, Parvin A, Islam MA, et al. The utility of bioremediation approach over physicochemical methods to detoxify dyes discharges from textile effluents: A comprehensive review study. Sustainable Chemistry and Pharmacy 2024;39:Article No. 101538.

Spagnuolo D, Iannazzo D, Len T, Balu AM, Morabito M, Genovese G, et al. Hydrochar from *Sargassum muticum*: A sustainable approach for high-capacity removal of Rhodamine B dye. RSC Sustainability 2023;1(6):1404-15.

Susanti E, Ristanti Widoretno M, Oktaviyani D, Sumi Lestari F, Muit N, Kurniawan R, et al. Sorption kinetics of heavy metals from aqueous solution using *Spirogyra* sp.: A microcosm study. LIMNOTEK Perairan Darat Tropis di Indonesia. 2023;29(1):Article No. 1190.

Tipnee S, Unpaprom Y, Ramaraj R, Tipnee S, Ramaraj R, Unpaprom Y. Nutritional evaluation of edible freshwater green macroalga *Spirogyra varians*. Emerging Topics in Life Sciences 2015;1(2):1-7.

Tones ARM, Eyng E, Zeferino CL, Ferreira S de O, Alves AA de A, Fagundes-Klen MR, et al. Spectral deconvolution associated to the Gaussian fit as a tool for the optimization of photovoltaic electrocoagulation applied in the treatment of textile dyes. Science of the Total Environment 2020;713:Article No. 136301.

Tsarpali M, Kuhn JN, Philippidis GP. Hydrothermal carbonization of residual algal biomass for production of hydrochar as a biobased metal adsorbent. Sustainability (Switzerland) 2022;14(1):Article No. 455.

Ullah F, Ji G, Irfan M, Gao Y, Shafiq F, Sun Y, et al. Adsorption performance and mechanism of cationic and anionic dyes by KOH activated biochar derived from medical waste pyrolysis. Environmental Pollution 2022;314:Article No. 120271.

Umesh AS, Puttaiahgowda YM, Thottathil S. Enhanced adsorption: Reviewing the potential of reinforcing polymers and hydrogels with nanomaterials for methylene blue dye removal. Surfaces and Interfaces 2024;51:Article No. 104670.

Vetrivel SA, Diptanghu M, Ebhin MR, Sydavalli S, Gaurav N, Tiger KP. Green algae of the genus *Spirogyra*: A potential absorbent for heavy metal from coal mine water. Remediation 2017;27(3):81-90.

Wang H, Chen C, Dai K, Xiang H, Kou J, Guo H, et al. Selective adsorption of anionic dyes by a macropore magnetic lignin-chitosan adsorbent. International Journal of Biological Macromolecules 2024;269(2):Article No. 131955.

Wibiyan S, Royani I, Ahmad N, Lesbani A. Assessing the efficiency, selectivity, and reusability of ZnAl-layered double hydroxide and *Eucheuma cottonii* composite in removing anionic dyes from wastewater. Inorganic Chemistry Communications 2024a;170:Article No. 113347.

Wibiyan S, Royani I, Lesbani A. Selective adsorption of cationic and anionic dyes using Ni/Al layered double hydroxide modified with *Eucheuma cottonii*. Indonesian Journal of Material Research 2024b;2(1):1-6.

Wibiyan S, Royani I, Lesbani A. Synthesis and performance of ZnAl@ layered double hydroxide composites with *Eucheuma cottonii* for adsorption and regeneration of Congo red dye. Indonesian Journal of Environmental Management and Sustainability 2024c;8(3):126-34.

Wibiyan S, Wijaya A, Siregar PMSBN. Adsorption of phenol using cellulose and hydrochar: Kinetic, isotherm, and regeneration studies. Indonesian Journal of Material Research 2023;1(2):61-7.

Wibowo YG, Syahnur MT, Al-Azizah PS, Arantha Gintha D, Lululangi BRG, Sudibyo. Phytoremediation of high concentration of ionic dyes using aquatic plant (Lemna minor): A potential eco-friendly solution for wastewater treatment. Environmental Nanotechnology, Monitoring and Management 2023;20:Article No. 100849.

Wierzbicka E, Kuśmierek K, Świątkowski A, Legocka I. Efficient rhodamine B dye removal from water by acid- and organo-modified halloysites. Minerals 2022;12(3):Article No. 350.

Wijaya A, Ahmad N, Hanum L, Melwita E, Lesbani A. *Spirogyra* sp. macro-algae-supported NiCr-LDH adsorbent for enhanced remazol red dye removal. Results in Surfaces and Interfaces 2025;18:Article No. 100427.

Wu J, Wang T, Li S, Tang W, Yu S, Zhao Z, et al. A green method to improve adsorption capacity of hydrochar by ball-milling: Enhanced norfloxacin adsorption performance and mechanistic insight. Carbon Research 2024;3(1):Article No. 60.

Yihunu EW, Minale M, Abebe S, Limin M. Preparation, characterization and cost analysis of activated biochar and hydrochar derived from agricultural waste: A comparative study. SN Applied Sciences 2019;1(8):Article No. 873.

Zhao Y, Qi K, Pan J. Efficient corn straw and poplar leaf biochar-based adsorbents for the eradication of methylene blue from aqueous solutions. Desalination and Water Treatment 2023;303:236-44.